UNIVERSITY OF MISKOLC
FACULTY OF MECHANICAL ENGINEERING AND INFORMATICS

NEW APPROACHES IN THE SIMULATION OF HEAT TRANSFER THROUGH BUILDING'S WALLS AND ROOFS

Booklet of PhD Theses

PREPARED BY:

Ali Habeeb Askar Al-Magsoosi

Mechanical Engineering Department (BSc),
Mechanical Engineering Department (MSc)

ISTVÁN SÁLYI DOCTORAL SCHOOL OF MECHANICAL ENGINEERING SCIENCES
TOPIC FIELD OF BASIC ENGINEERING SCIENCES
TOPIC GROUP OF TRANSPORT PROCESSES AND MACHINES

HEAD OF DOCTORAL SCHOOL
Dr. Gabriella Bognár
DSc, Full Professor

HEAD OF TOPIC GROUP
Dr. László Baranyi
Full Professor

SCIENTIFIC SUPERVISOR
Dr. Endre Kovács
Dr. Betti Bolló

Miskolc
2025

JUDGING COMMITTEE

Chair:

Secretary:

Members:

OFFICIAL REVIEWERS

1. INTRODUCTION

The rise of smart technologies has transformed energy optimization in buildings, which consume 40% of primary energy and contribute 24% to greenhouse gas emissions. This thesis examines smart home technologies, energy efficiency, and thermal comfort, focusing on heat transfer in building envelopes. Predicting energy needs during design is key to optimizing energy use and economic outcomes [1]. The International Energy Agency notes the construction sector accounts for over a third of global energy consumption and 40% of CO_2 emissions. In Hungary, fossil fuels dominate the energy supply, but solar PV installations are growing to meet clean energy goals by 2030 [2].Building envelopes, especially walls, are critical for reducing heat loss, which accounts for 35% of a home's energy loss. Enhancing insulation and using smart materials can improve efficiency. Thermal bridges, which increase heat loss, require integrated thermal and structural design [3]. This study explores energy renovation techniques for existing buildings to boost efficiency and sustainability.

Energy efficiency in buildings is vital for a sustainable economy, with the construction sector offering significant potential to reduce energy use and emissions. Heat transfer calculations guide building design, estimating energy loss through conduction in walls, roofs, and floors. Wall conduction, influenced by thickness and insulation, responds to weather conditions, impacting thermal comfort and energy consumption [4]. Innovative wall designs, like passive solar and lightweight concrete, enhance efficiency, while high R-values reduce heat loss [5]. However, high humidity can cause condensation, risking microbial growth. Roofs, critical for shielding against solar radiation, benefit from insulation and reflective coatings to minimize heat gain. In tropical climates, passive cooling techniques, like ventilated roofs, improve comfort. Fenestration, including advanced glazing technologies, optimizes thermal performance and lighting. These strategies—improved insulation, innovative walls, and efficient roofing—collectively lower energy demands, fostering sustainability in buildings [6].

Analytical solutions for homogeneous systems are used to validate numerical methods, particularly for one-dimensional multilayer problems in building envelope heat gain, loss, and storage [7]. However, most building heat conduction issues are multi-dimensional and transient, with varying material properties, requiring numerical simulations. Thermal analysis examines temperature distributions, fluxes, and heat capacities, often using numerical methods for complex, non-homogeneous scenarios [8]. Analytical solutions are precise for simple geometries, but numerical integration is needed when material properties vary spatially. Newton's law of cooling and Stefan–Boltzmann's law describe convective and radiative heat transfer, incorporated into numerical models like finite difference schemes (FDM). Implicit FDM methods offer stability but are computationally slow for multi-dimensional problems, while explicit methods, though faster and parallelizable, are conditionally stable under the CFL limit [9]. Semi-explicit or semi-implicit

methods balance stability and speed, with algorithms like the leapfrog–hopscotch (LH) method excelling in heat conduction simulations. Studies show LH, Dufort–Frankel, and hopscotch methods perform well, especially for stiff systems, allowing large time steps without stability issues [10]. These methods effectively model convection and radiation in building walls across seasons. Developing new algorithms for diffusion-reaction equations with time- and space-dependent coefficients remains a key focus.

In my research, I collaborated with my supervisors and colleagues to explore and enhance families of novel and traditional explicit methods for solving linear and nonlinear heat conduction equations. These methods were developed based on innovative approaches. Specifically, I adapted successful techniques, such as the pseudo-implicit and Leapfrog hopscotch methods, to scenarios involving heat transfer through convection and nonlinear radiation (like Stefan-Boltzmann-type radiation). These adaptations addressed real-world heat transfer challenges in building environments. Additionally, I conducted a comparative analysis of my findings with those obtained from neural networks

Diffusion of particles and Fourier-type heat conduction are omnipresent mass or energy transport processes.

$$\frac{\partial u}{\partial t} = \alpha \nabla^2 u + q \tag{1.1}$$

In the simplest linear case, they are described by the following partial differential equation (PDE):

$$\frac{\partial u(x,t)}{\partial t} = \alpha \frac{\partial^2 u(x,t)}{\partial x^2} + q\,, \tag{1.2}$$

where $x, t \in \mathbb{R}$ are the independent variables, $u = u(x,t)$ is the unknown concentration of particles or the temperature in the case of heat transfer, and α is the coefficient of (thermal) diffusivity. The thermal diffusivity of a material can be given as $\alpha = k/(c\rho)$, where $c = c(\vec{r},t)$, $k = k(\vec{r},t)$, and $\rho = \rho(\vec{r},t)$ are the specific heat, the heat conductivity, and the density of the material, respectively. If these coefficients depend on space, one has to use the more general equation

$$\frac{\partial u}{\partial t} = \frac{1}{c\rho}\nabla\left(k\nabla u\right), \tag{1.3}$$

where it is assumed that the c and ρ functions are positive. This equation is now valid for more than one space dimension.

The heat conduction Eq. (1.2) can be extended to include heat convection, radiation, and source terms are added to the heat conduction Eq.(1.1). In the case of Eq. (1.2) in one space dimension, applying the most common central difference equation

$$\frac{\partial^2}{\partial x^2}u(x_i) \approx \frac{\dfrac{u(x_{i+1})-u(x_i)}{\Delta x} + \dfrac{u(x_{i-1})-u(x_i)}{\Delta x}}{\Delta x} = \frac{u_{i-1}-2u_i+u_{i+1}}{\Delta x^2}\,, \tag{1.4}$$

which is second order in Δx, where $i = 1,\ldots,N$ and N is the overall number of nodes. By applying this, in one space dimension, I am able to derive the spatially discretized form of the heat transfer Eq. (1.1) in one space dimension as follows:

$$\frac{du_i}{dt} = \alpha \frac{u_{i-1} - 2u_i + u_{i+1}}{\Delta x^2} + q - Ku_i - \sigma u_i^4 \,. \tag{1.5}$$

Now, let us demonstrate the discretization of the heat transfer equation assuming that the variables α, k, c, and ρ, which describe the properties of materials, are functions of space rather than fixed values. In one space dimension, I now have to deal with the following instead of the term $\alpha \nabla^2 u$ for homogeneous materials:

$$\frac{1}{c(x)\rho(x)} \frac{\partial}{\partial x}\left(k(x) \frac{\partial u}{\partial x} \right) . \tag{1.6}$$

I discretize the function k, and at the same time the space derivatives in Eq. (1.6) by the standard central difference formula to obtain:

$$c(x_i)\rho(x_i) \left.\frac{\partial u}{\partial t}\right|_{x_i} = \frac{1}{\Delta x}\left[k\left(x_i + \frac{\Delta x}{2} \right) \frac{u(x_i + \Delta x) - u(x_i)}{\Delta x} + k\left(x_i - \frac{\Delta x}{2} \right) \frac{u(x_i - \Delta x) - u(x_i)}{\Delta x} \right]. \tag{1.7}$$

Equations (1.6) and (1.7) are based on the node-picture, typically used by mathematicians. Instead of node-variables, let us introduce cell variables to arrive at a resistance-capacitance-type model of heat conduction. It means that u_i, c_i, and ρ_i are the approximation of the average temperature, specific heat, and density of cell i, by their value at the cell centre. Furthermore, $k_{i,i+1}$ is the heat conductivity between cell i and its (right) neighbour, estimated by its value at the border of the cells. Now the previous formula will have the form:

$$\frac{du_i}{dt} = \frac{1}{c_i \rho_i \Delta x}\left(k_{i,i+1} \frac{u_{i+1} - u_i}{\Delta x} + k_{i-1,i} \frac{u_{i-1} - u_i}{\Delta x} \right) + q - Ku_i - \sigma u_i^4 \,. \tag{1.8}$$

As a generalization of Eq. (1.8) one may construct the ODE system for the time derivative of the cell variables for a generic grid by using the above approximations as follows:

$$\frac{du_i}{dt} = \sum_{j \neq i} \frac{u_j - u_i}{R_{i,j} C_i} + q - Ku_i - \sigma u_i^4 \,. \tag{1.9}$$

The set of ordinary differential equations (ODEs) shown here can be used with a lot of different grids, even ones that are not structured and have cells that are different sizes, shapes, and properties. It is important to note that uneven discretization may potentially compromise spatial accuracy. However, for the purposes of this work, I have chosen to exclusively utilize cells of a rectangular configuration.

2. METHODOLOGY OF THE STUDY

My objective is to refine and optimize numerical methods to effectively analyze heat transfer in building components, enabling optimization of building envelopes from both thermodynamic and economic perspectives. The research is structured into three key areas. First, I systematically evaluate nine numerical algorithms, assessing their stability and accuracy, develop a pseudo-implicit algorithm, investigate free convection and radiation terms using the leapfrog-hopscotch method, and compare numerical approaches for diffusion-reaction partial differential equations (PDEs). Second, I apply neural networks to predict building energy performance, validate models, and simulate the thermal behavior of building walls using the leapfrog-hopscotch method as the recommended approach. Third, I optimize roof inclination angles for energy efficiency across various climates and enhance roof designs by incorporating additional insulation and Trombe roof systems. These efforts aim to advance energy-efficient building design through rigorous computational analysis and innovative optimization strategies.

2.1 Some Explicit Methods

2.1.1 The Leapfrog–Hopscotch method

The leapfrog-hopscotch (LH) method [11]. We have a structure consisting of two half and several full time steps. The calculation starts again by taking a half-sized time step for the odd nodes using the initial values Stage 0 (not repeated, green box), which uses $\theta=0$. Then, for the even and odd nodes, full-time steps are taken strictly alternately until the end of the last timestep, The intermediate stages as well as the last stage (light and dark orange boxes) use $\theta=1/2$ Figure 2.1. I used only the best already proven combination of formulas (L2 in [11]), which means that $\theta=0$ and $\theta=1/2$.

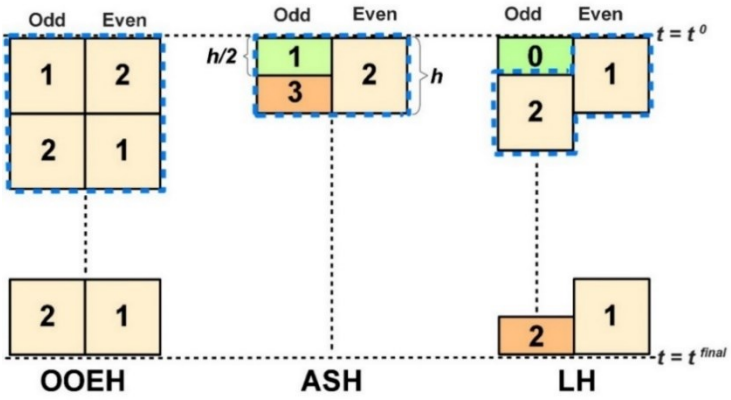

Figure 2.1. Hopscotch-type space-time structures. The time elapses from the top $\left(t=t^{0}\right)$ to the bottom $\left(t=t^{\text{fin}}\right)$.

2.1.2 The Dufort–Frankel (DF) algorithm

This method can be obtained from the so called leapfrog explicit scheme by a modification [12] (p. 313). It is a known explicit unconditionally stable scheme that has the formula in the special and general case:

$$u_i^{n+1} = \frac{(1-2r)u_i^{n-1} + 2r\left(u_{i-1}^n + u_{i+1}^n\right)}{1+2r} \text{ and } u_i^{n+1} = \frac{(1-r_i)u_i^{n-1} + 2A_i}{1+r_i}.$$

As one can see, it is a one-stage but two-step method (the formula contains u_i^{n-1}), which is not a self-starter, so another method must be applied to start the method by the calculation u_i^1. For this purpose, we apply the UPFD formula twice (with halved time step size).

2.2 Comparison the ARE errors between positivity preserving methods as a function of ΔtMAX and stiffness ratio

Figure 2.2. and Figure 2.3 show *ARE* errors as a function of Δt_{MAX} and stiffness ratio, respectively. I note the stiffness ratio affected the accuracy of methods when they increased, so the accuracy becomes worse compared to the cases of small stiff ratios.

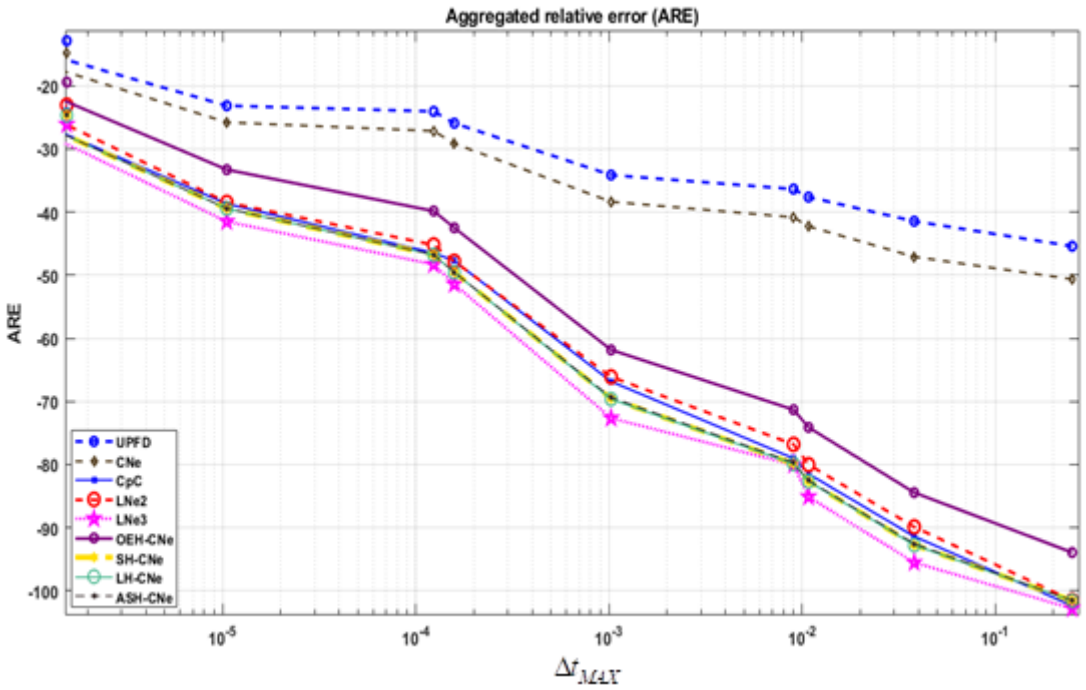

Figure 2.2. The ARE errors as a function of Δt_{MAX} in the case of the UPFD, CNe, CpC, LNe2, LNe3, the OEH-CNe, the SH-CNe, the LH-CNe and the ASH-CNe methods.

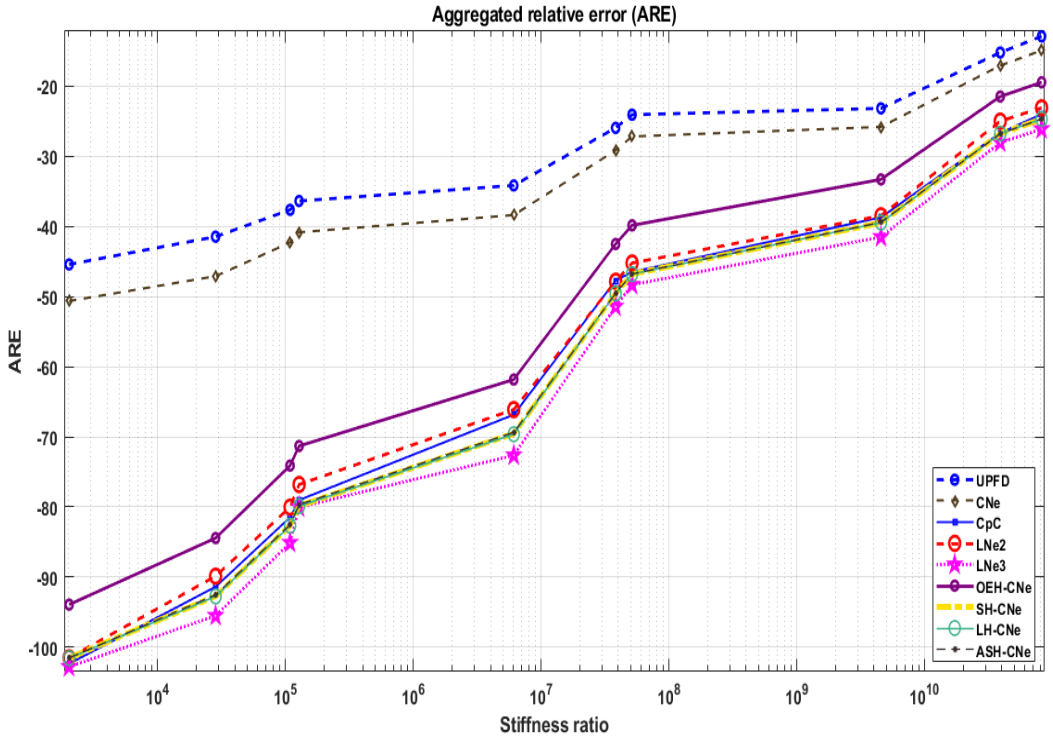

Figure 2.3. The ARE errors as a function of Stiff Ratio in the case of the UPFD, CNe, CpC, LNe2, LNe3, the OEH-CNe, the SH-CNe, the LH-CNe and the ASH-CNe methods.

I summarize the ARE error quantities, for both case studies in Table 2.1.

Table 2.1. ARE (average relative error) quantities of different explicit stable algorithms.

Numerical Method	ARE (Mildly Stiff)	ARE (Very Stiff)
UPFD	–37.4544	–23.1613
CNe	–42.0347	–25.9
CpC	–80.778	–40.07
LNe2	–79.6922	–39.228
LNe3	–84.346	–43.75
OEH-CNe	–72.9442	–35.09
SH-CNe	–81.467	–41.4367
LH-CNe	–81.4812	–41.428
ASH-CNe	–81.376	–41.394

2.3 PI Algorithms Comparison with Other Methods for a Large System with Strong Nonlinearity

In this case study, I set $K_i = 3 \times rand$, $q_i = 2 \times rand$ and $\sigma = 1000$. The latter coefficient has been chosen so large because I would like to demonstrate the performance of the new method for a strongly nonlinear case, but the values of the variable u are typically between zero and one, thus their fourth power is usually a rather small number. I solve Eq. (1.1) in a 2-D, rectangle-structured

mesh the size of the system is fixed to $N_x = 100$ and $N_z = 120$, thus the total cell number is 12,000. Randomly generated cell capacities and thermal resistances,

$C_{\mathrm{i}} = 10^{(\alpha_C - \beta_C \times rand)}$, $R_{\mathrm{x,i}} = 10^{(\alpha_{Rx} - \beta_{Rx} \times rand)}$, $R_{\mathrm{z,i}} = 10^{(\alpha_{Rz} - \beta_{Rz} \times rand)}$,

I give new values to the α and β exponents:

$\alpha_C = 3,\ \beta_{\mathrm{C}} = 6,\ \alpha_{Rx} = \alpha_{Rz} = 3,\ \beta_{Rx} = \beta_{Rz} = 0$.

I calculate the stiffness ratio and the CFL limit in two different ways, both of them without taking into account the nonlinear term. If I use the full M matrix, I obtain that the stiffness ratio is 7.7×10^5 much smaller than in the previous case, while the CFL limit for the standard FTCS was $\Delta t_{MAX}^{EE} = 9.76 \times 10^{-4}$, which, I stress again, holds for the Heun method as well. If I use only the M^D matrix instead of M, the stiffness ratio is 6.8×10^9, while the CFL limit is $\Delta t_{MAX}^{EE} = 9.75 \times 10^{-4}$. The reason behind these numbers is that the eigenvalues close to zero have been significantly increased (in absolute value) by the new reaction term while those with large absolute values remained almost the same. All other parameters and circumstances, such as the size of the system and the range of the initial values are the same as in the previous subsection. I note that I were not able to adapt our previous methods CNe, LNe and CpC for the $K \neq 0, \sigma \neq 0$ case, nor when the advection term is present, without losing their order of convergence (that is why I started to develop the current methods), thus they are not presented in this and the next subsection. In Figure 2.4 the energy and the average errors are presented as a function of the time step size and Figure 2.5 the total running time, respectively.

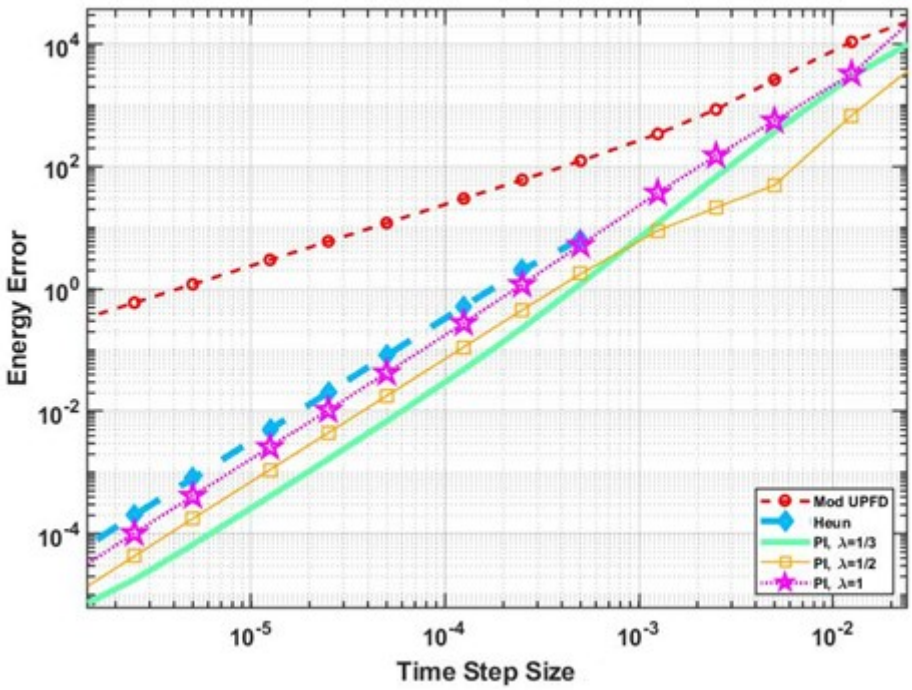

Figure 2.4. Energy errors as a function of the time step size for the second (very stiff) system, in the case of the UPFD Algorithm 2, the Heun method and the new PI algorithms.

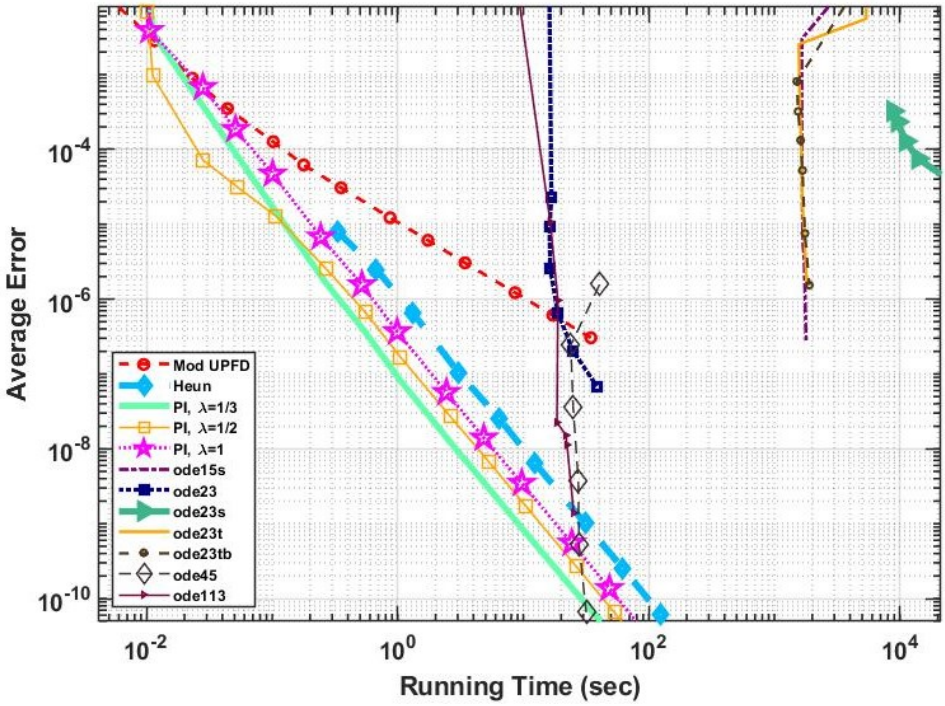

Figure 2.5. Energy (average) errors as a function of the running time for the second (very stiff) system, in the case of the new algorithms and some other methods.

2.5 Results for the Cross-section of the Insulated Wall with Thermal Bridging

Part I: The equidistant mesh. Here the initial and boundary conditions of point (B) are applied to the multilayer wall. The maximum errors are plotted in Figure 2.6. The temperature distribution contour for final time moments is shown in Figure 2.8. The temperature on the right side of the wall is rising due to the higher outside temperature, but the insulator allows this heat to enter the wall at a very slow rate.

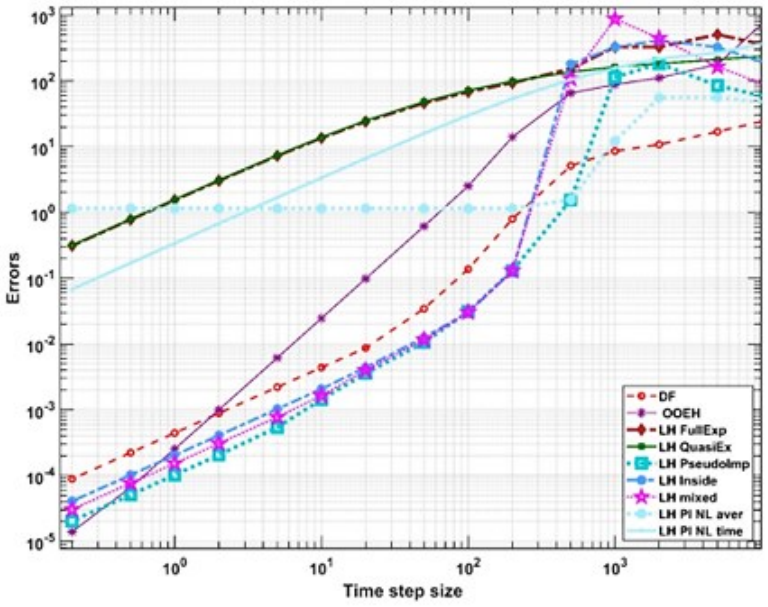

Figure 2.6. The maximum errors as a function of h for the equidistant mesh (Part I) in the case of convection and radiation boundary conditions.

Part II: non-equidistant mesh, is the same as in (Part I). The errors are presented in Figure 2.7.

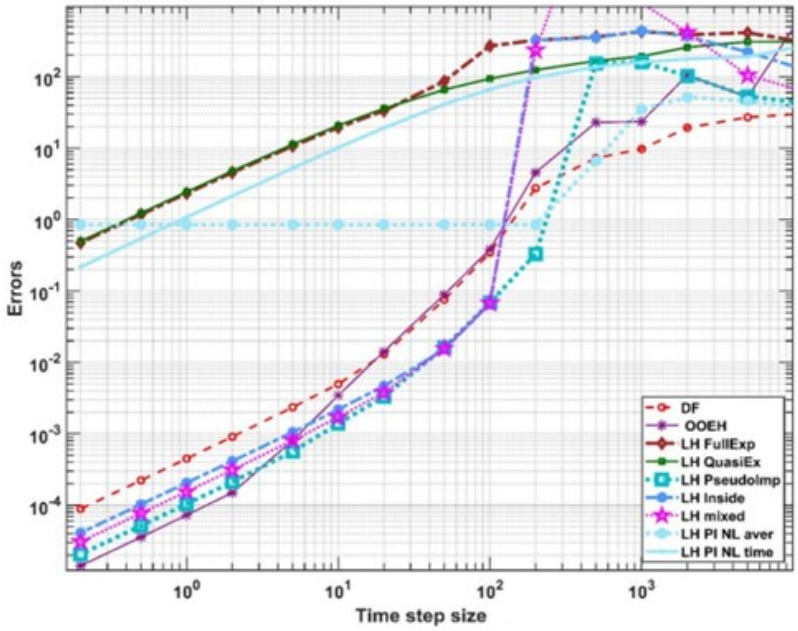

Figure 2.7. The maximum errors vs. the time step size h for the non-equidistant mesh (Part II) in the case of convection and radiation boundary conditions.

while the temperature contours are presented in Figure 2.8, the non- equidistant mesh, in case of the multilayer cross-sectional area. The numbers on the vertical and horizontal axes of the contours are the coordinates in cm units.

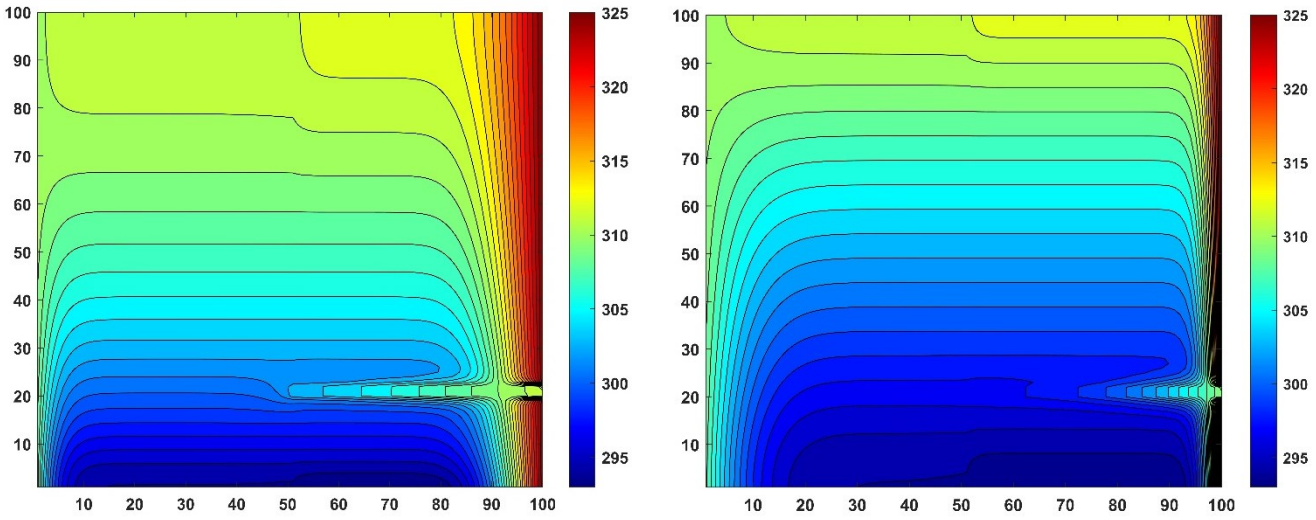

Figure 2.8. The temperature distribution contour in Kelvin for the final time (left) in the case of (Part I) (equidistant mesh) and final time (right) (Part II).

2.6 Results for the Surface of the Wall

Figure 2.9 shows the temperature distribution contour in Kelvin units for the surface area. The figure shows that in the case of the insulator (right-hand side of the figure), heat can hardly flow

from the top of the figure to the bottom, so there are large temperature gradients. Moreover, because the heat capacity of the insulation layer is smaller than that of the brick layer, its temperature increases faster from the original 270 K.

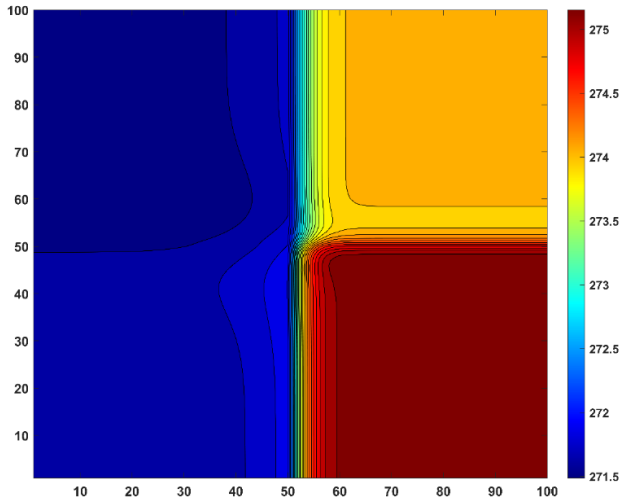

Figure 2.9. The temperature distribution contour in Kelvin units for the surface area (upper half) constant convection and (lower half) the convection changes with time depending on weather data.

The maximum errors of the cell-temperatures at the final time as a function of time step size are shown in Figure 2.10 for the systems 100 by 100. Figure 2.11 shows the running time for the system 100 by 100. I use many time steps for the explicit methods (LH and DF) and less for the implicit methods because they are much slower, and I see that LH and DF are faster and more accurate.

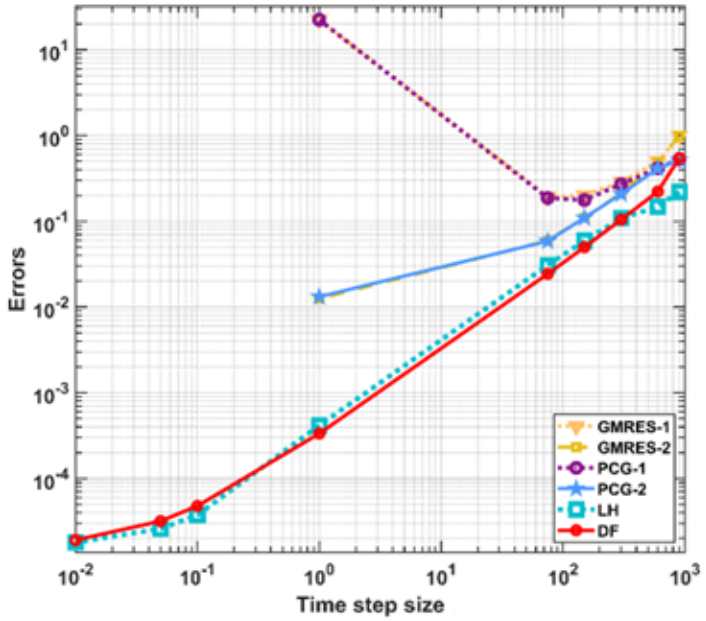

Figure 2.10. The maximum errors as a function of the time step size h for the examined methods for the 100 by 100 system.

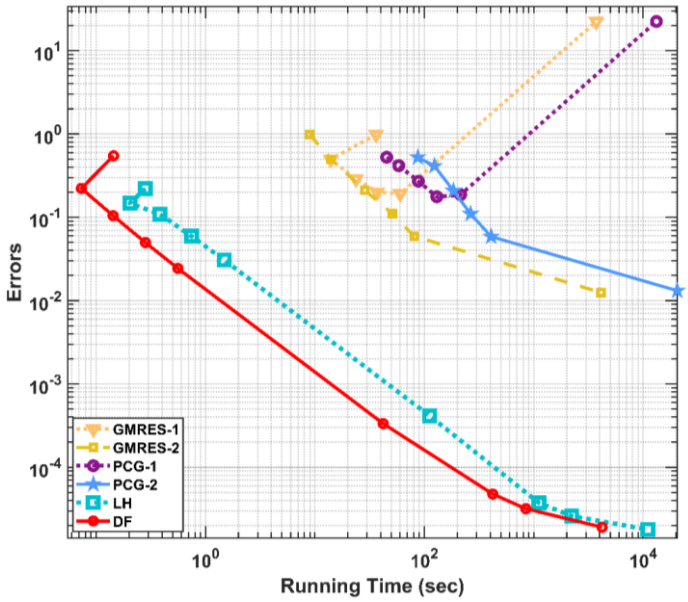

Figure 2.11. The maximum errors as a function of the running time for the tested methods for the 100 by 100 system.

2.6.1 Applying MLP and RB neural networks

To validate my results, I compared the predicted data with the experimental data collected by HAP, based on the CL and HL parameters. I used R^2 as a criterion for the predicted data. Figure 2.12 shows the comparison of the predicted data with the experimental data. The results indicate that the LM model has the best prediction performance among all models. The analytical results are also in good agreement with the experimental data, which confirms the reliability of the ANN training process using different algorithms. The RB model, however, has the lowest prediction accuracy and fails to optimize the ANN parameters effectively. The SCG model can be a suitable alternative to the LM model and provides accurate results and predictions, but it is still less accurate than the LM model.

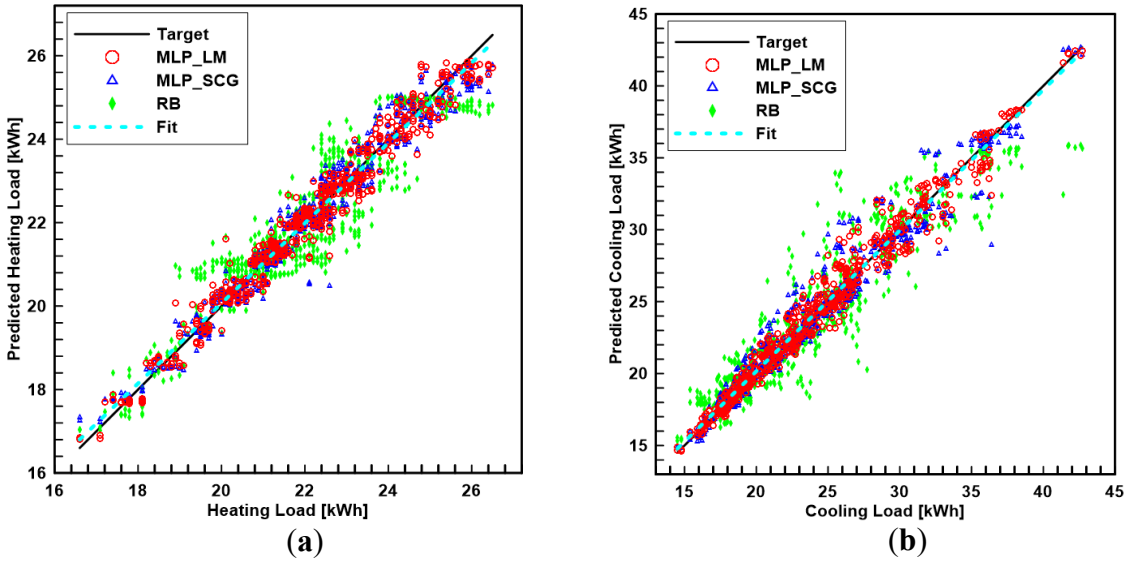

Figure 2.12. The result of R^2 values for the data predicted by three neural networks: MLP_LM, MLP_SCG, and RB (**a**) for the heating load and (**b**) for the cooling load.

2.6.2 Result for the Simulation of the Wall

2.6.2.1 Winter Simulation

This section presents the results of a simulation of heat transfer and temperature distribution in a four-layered wall (gypsum plaster, heavy weight concrete, insulation, and face brick) during the winter season (December). The simulation shows how the temperature varies across the layers and how much heat is lost from the inside to the outside of the wall per meter square. Figure 2.13 shows the temperature distribution at the boundary surfaces of the layers when the wall faces North.

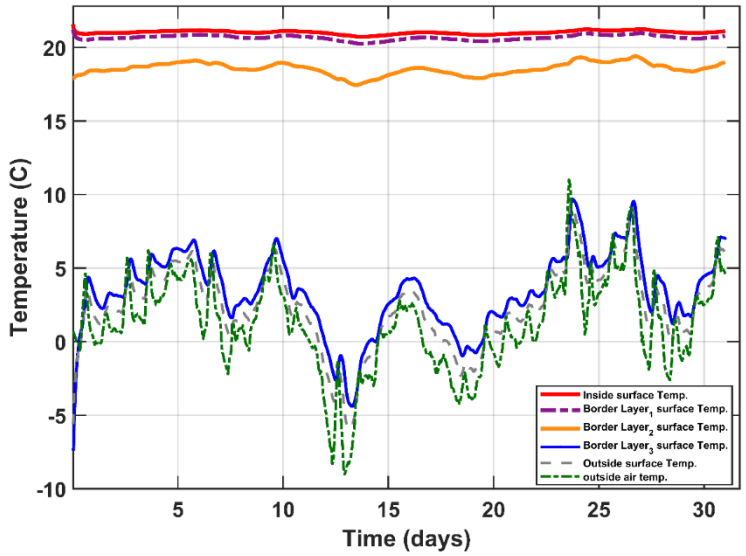

Figure 2.13. The temperature distribution in °C as a function of time in days for the four-layer wall facing North.

Figure 2.14 shows that the heat loss per meter squared is the highest for the wall facing North and lowest for the wall facing South.

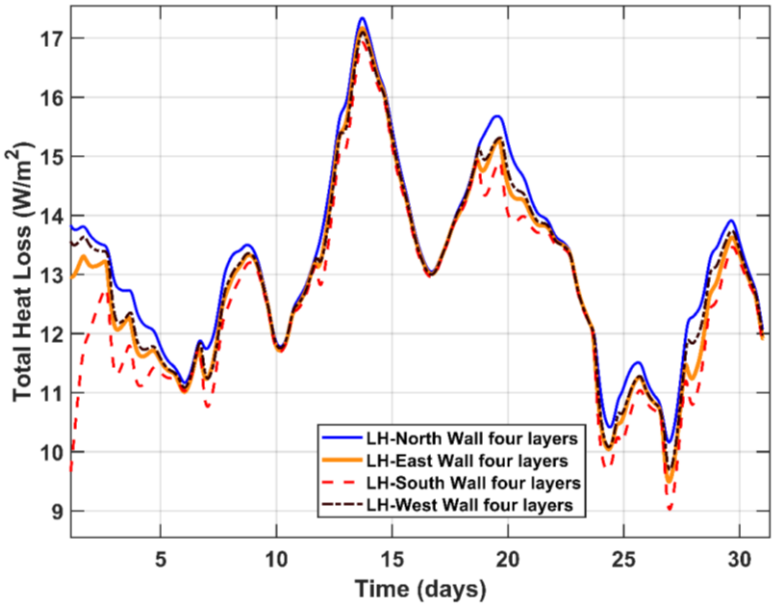

Figure 2.14. Total heat loss distribution in W/m^2 as a function of time in days for the wall simulation facing North, East, South, and West.

2.6.2.2 Summer Simulation

This section shows the results of a simulation of heat transfer and temperature distribution in the four-layered wall during the summer season (July). The simulation shows how the temperature varies across the layers and how much heat is gained from the outside to the inside of the wall per meter squared. Figure 2.15 shows the temperature distribution at the boundary surfaces of the layers when the wall faces North.

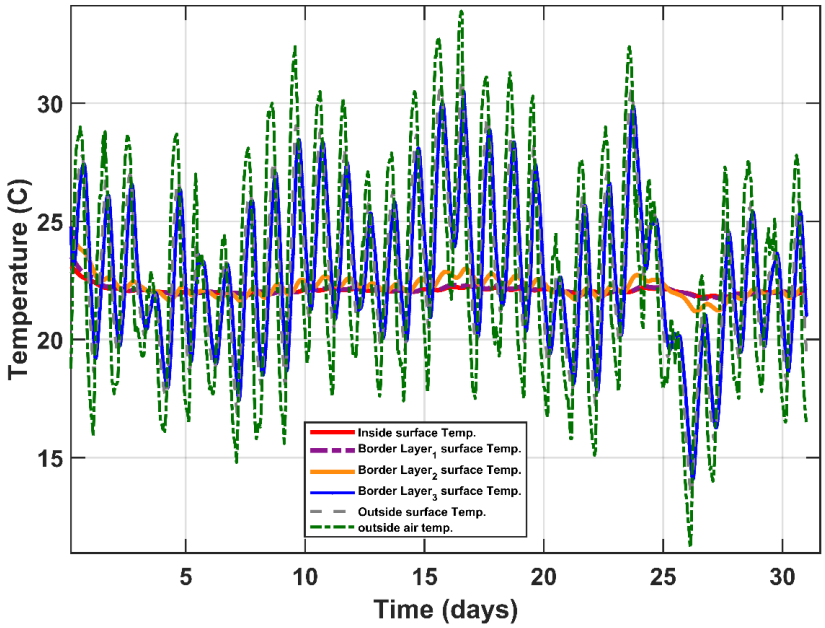

Figure 2.15. The temperature distribution in °C as a function of time in days for the four-layer wall facing North.

Figure 2.16 illustrates that the heat gain per meter squared is lowest for the wall facing North and highest for the wall facing South, due to there being no radiation on the north side in the daytime.

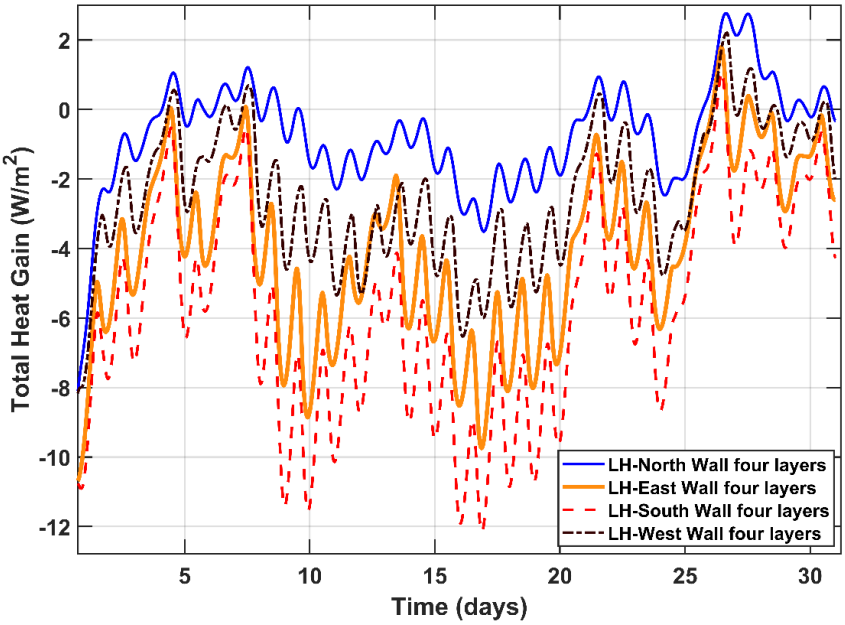

Figure 2.16. Total heat gain distribution in W/m^2 as a function of time in days for the wall simulation facing North, East, South, and West.

2.7 Comparative Analysis Between The Optimal Models And The Horizontal Roof

I conduct a comparative analysis between the optimal models and the horizontal model in Figure 2.17. Specifically, I take into account the orientations facing east and west, integrating them into the load calculations for the north and south directions. The resulting combined load is subsequently compared to the load associated with the horizontal configuration. Although an inclined roof has a larger surface area than a horizontal roof, it has reduced heat loss and gain. This is attributed to a shorter duration of exposure to solar radiation, resulting in lower heat gain, and to the consistent thermal convection on the sides of the inclined roof. Additionally, when exposed to solar radiation, it stores energy and re-radiates it, which minimizes heat loss compared to a horizontal roof. Consequently, the inclined design offers improved thermal performance despite its increased surface area.

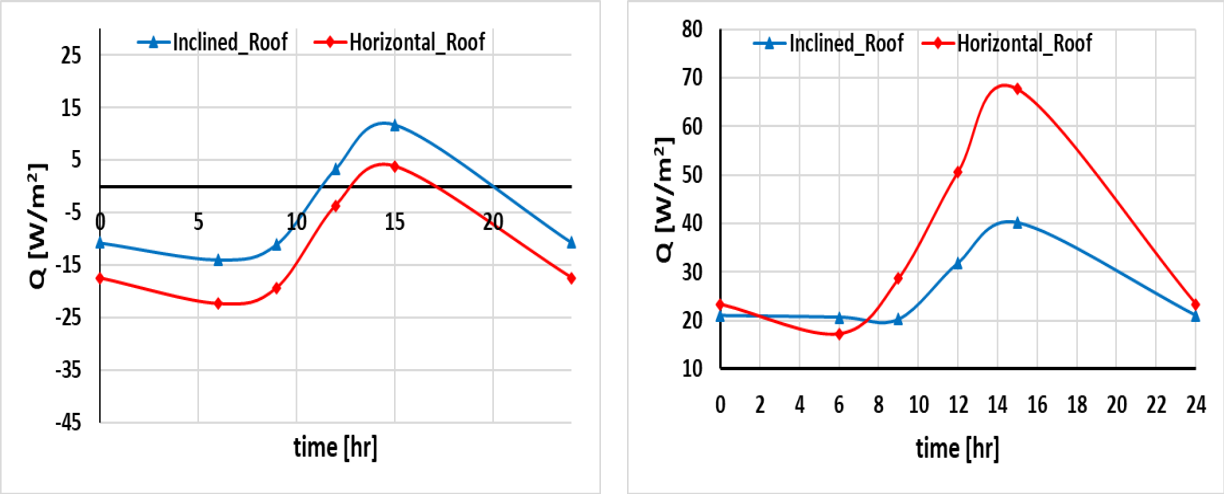

winter **summer**

Figure 2.17. Roof heat loss and gain with time on left side winter season and right-side summer season.

Figure 2.18 illustrates the optimal roof contour for temperature regulation during both winter and summer seasons. The subsequent two figures demonstrate the enhancements achieved by incorporating a Trombe wall and insulation on the effective side of the roof for both seasons.

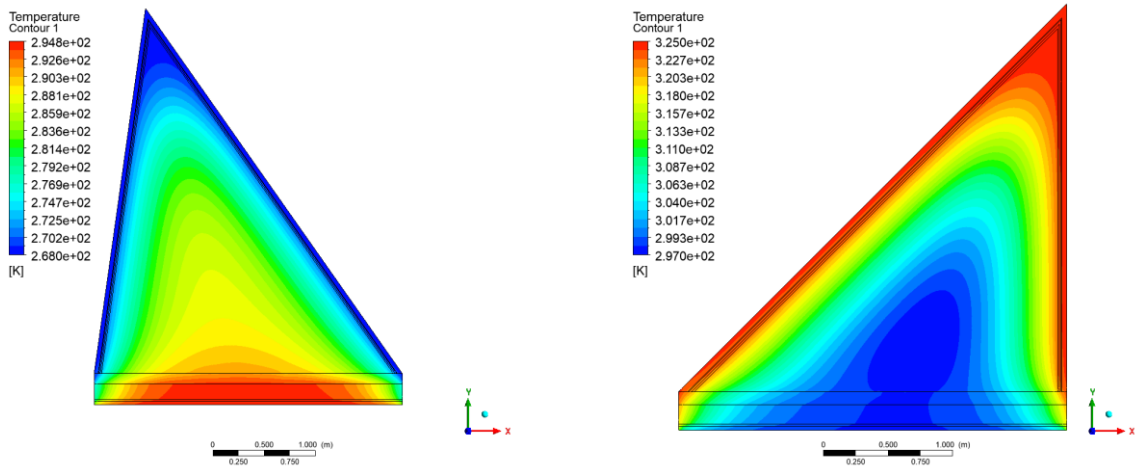

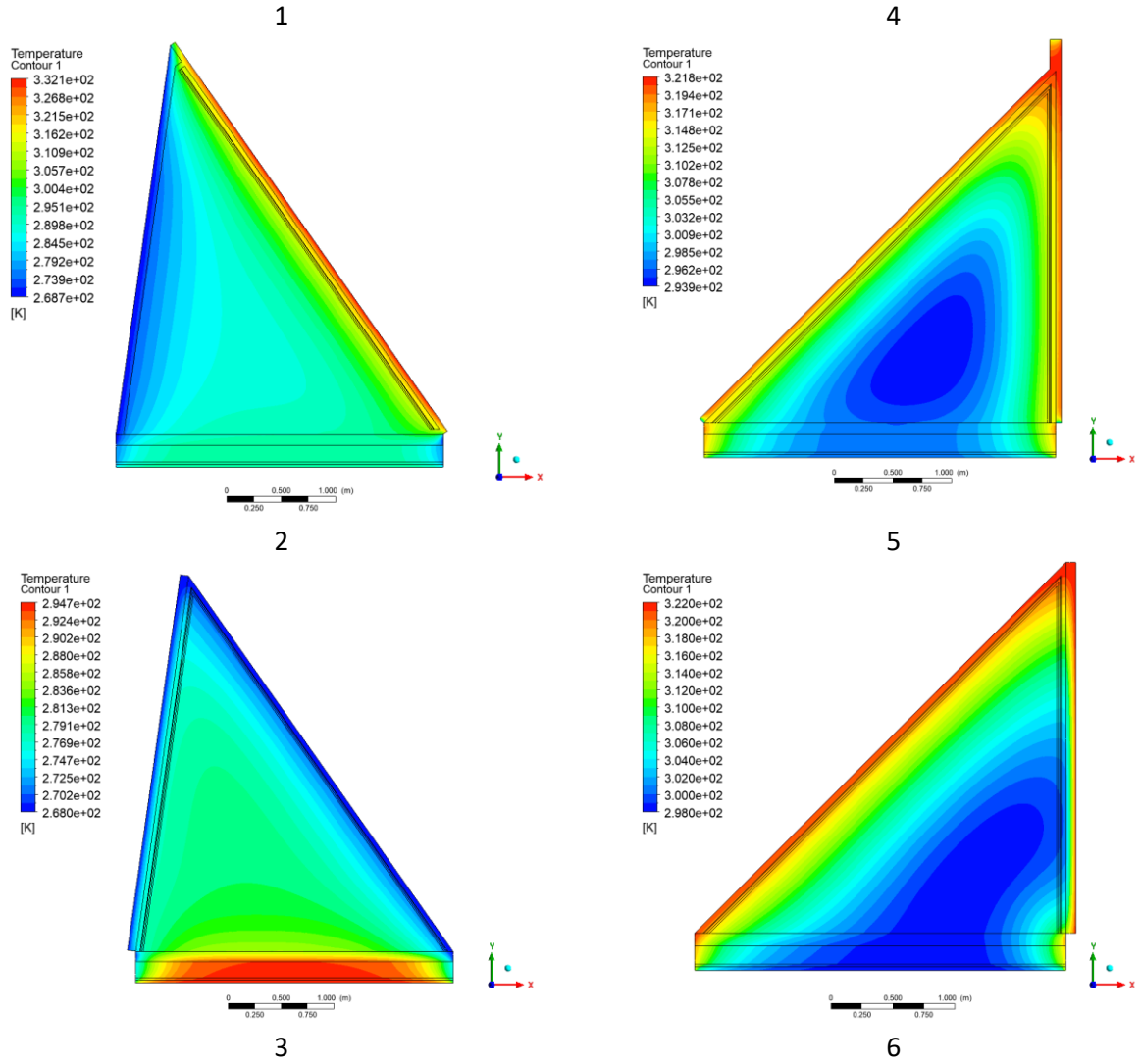

Figure 2.18. Contour of temperature for the optimal roof cases, Trombe and with insulation on effective side on left side winter season Hungary, Miskolc and right-side summer season Baghdad, Iraq.

3. NEW SCIENTIFIC RESULTS – THESES

T1. I analyzed nine numerical algorithms for solving the heat equation, focusing on positivity-preserving methods stable across time step sizes and system stiffness. The study tested 2500-cell, two-dimensional stiff systems with random, discontinuous parameters. I compared accuracy and CPU efficiency, finding the 3-stage LNe3 and LH-CNe methods most accurate. I examined how increasing stiffness ratios, decreasing CFL limits, and varying spatial anisotropy affected accuracy. The study assessed performance with growing horizontal-vertical cell dimension differences. I recommended optimal methods for scenarios like OEH structure, unstructured meshes, and highly anisotropic systems, aiming to guide effective positivity-preserving method selection. [13].

T2. I developed a novel, fully explicit, stable numerical algorithm for time-dependent diffusion equations with linear and nonlinear reaction terms. Based on the UPFD idea and theta-formula, it's second order in time step size and unconditionally stable for linear cases. It outperforms other methods and MATLAB routines in accuracy and stability for nonlinear cases, though not positivity-preserving. Stable for large time steps even with strong nonlinearity, it's easy to implement and suitable for unstructured grids. This pseudo-implicit algorithm combines key advantages of explicit and implicit methods.[14].

T3. I optimized the leapfrog-hopscotch method for the heat conduction equation, focusing on free convection and radiation terms. Best results treat convection 50% at old- and new-time levels, ensuring stability and second-order temporal convergence. The radiation term is best handled pseudo-implicitly for excellent stability. The algorithm performs well under low CFL limits. [15].

T4. I studied a diffusion-reaction PDE with a linear reaction term and space-time-dependent nonlinear coefficients. Nine numerical algorithms reproduced these, with Dufort-Frankel and leapfrog-hopscotch explicit schemes outperforming standard explicit and implicit methods. In a 2D case simulating wall surface temperature with wind-driven forced convection and rapidly varying material properties, explicit stable methods proved more efficient than implicit ones, with efficiency expected to grow with system size. [16].

T5. I compared MLP and RB neural networks using LM, SCG, and RB algorithms to predict heating and cooling loads in Miskolc, Hungary residences. The MLP with LM algorithm excelled in accuracy and error reduction. I also studied a four-layered wall's thermal behavior across orientations in winter and summer using the leapfrog-hopscotch finite difference algorithm. Insulation and orientation significantly affect thermal performance, with North-facing walls optimal in summer and South-facing in winter. Steady-state calculations overestimate winter heat loss and variably estimate summer heat gain. [17].

T6. I studied heat loss and gain in inclined roofs in Miskolc (cold winters) and Baghdad (hot summers). In Miskolc, optimal roof angles of 82° south and 55° north minimized heat loss. In Baghdad, 90° south and 45° north reduced heat gain. Trombe wall systems cut heat gain from 29.939 to 16.234 W/m², and insulating the active roof side lowered it to 23.997 W/m² in summer. Winter heat loss in Miskolc was 24.43, 21.77, and 20.91 W/m². [18] [19].

4. LIST OF PUBLICATIONS RELATED TO THE TOPIC OF THE RESEARCH FIELD

(1) A. H. Askar, E. Kovács, and B. Bolló, “Prediction and Optimization of Thermal Loads in Buildings with Different Shapes by Neural Networks and Recent Finite Difference Methods,” Buildings, vol. 13, no. 11, p. 2862, 2023.

(2) A. Ali Habeeb, Nagy, Ádám, Barna, Imre Ferenc and Kovács Endre, “Analytical and Numerical Results for the Diffusion-Reaction Equation When the Reaction Coefficient Depends on Simultaneously the Space and Time Coordinates,” 2023.

(3) Askar, A.H.; Omle, I.; Kovács, E.; Majár, J. Testing Some Different Implementations of Heat Convection and Radiation in the Leapfrog-Hopscotch Algorithm. Algorithms 2022.https://doi.org/10.3390/a15110400.

(4) H. K. Jalghaf, E. Kovács, J. Majár, Á. Nagy, and A. H. Askar, “Explicit stable finite difference methods for diffusion-reaction type equations,” Mathematics, vol. 9, no. 24, p. 3308, 2021.

(5) Omle, I.; Askar, A.H.; Kovács, E.; Bolló, B. Comparison of the Performance of New and Traditional Numerical Methods for Long-Term Simulations of Heat Transfer in Walls with Thermal Bridges. Energies 2023, 16, 4604. https://doi.org/10.3390/en16124604.

(6) A. H. Askar, E. Kovács, and B. Bolló, “ANN Modeling for Thermal Load Estimation in a Cabin Vehicle,” in Vehicle and Automotive Engineering 4: Select Proceedings of the 4th VAE2022, Miskolc, Hungary, Springer, 2022, pp. 357–373.

(7) Omle, I.; Askar, A.H.; Kovács, E. “Systematic testing of explicit positivity preserving algorithms for the heat-equation”. https://doi.org/10.28919/jmcs/7407.

(8) Omle, Issa, Ali Habeeb Askar, and Endre Kovács. "Optimizing the Design of Container House Walls Using Argon and Recycled Plastic Materials." *Buildings* 14, no. 12 (2024): 3944.

(9) A. A. Habeeb, K. Endre, and B. Betti, “Multi objective optimization for house roof using artificial neural network model,” Multidiszciplináris Tudományok, vol. 13, no. 2, pp. 11–25, Dec. 2023, doi: 10.35925/J.MULTI.2023.2.2.

(10) Abed, H. H., Omle, I., Askar, A. H., & Kovács, E. (2023). Experimental Study of the Stability and Thermophysical Properties for Different Particle Size of Al2o3-H2o Nanofluid. Journal of Engineering Science and Technology, 18(6), 2793-2808.

(11) Omle, I.; Askar, A.H.; Kovács, E.; "Impact of Wall Roughness Elements Type and Height on Heat Transfer Inside a Cavity". Pollack Periodica (2024). DOI:10.1556/606.2024.00986

(12) Habeeb, A. A., Hazim, A., Endre, K., & Károly, J. (2021). A new method to predict temperature distribution on a tube at constant heat flux. Multidiszciplináris Tudományok, 11(5), 363–372. https://doi.org/10.35925/J.MULTI.2021.5.40.

(13) Hazim, A., Habeeb, A. A., Károly, J., & Endre, K. (2021). Interpolated spline method for a thermal distribution of a pipe with a turbulent heat flow. Multidiszciplináris Tudományok, 11(5), 353–362. https://doi.org/10.35925/J.MULTI.2021.5.39.

(14) Jalghaf, H. K., Askar, A. H., Albedran, H., Kovács, E., & Jármai, K. (2023). Comparative study of different meta-heuristics on optimal design of a heat exchanger. Pollack Periodica, 18(2), 119–124. https://doi.org/10.1556/606.2022.00543.

(15) Askar, Ali Habeeb, Issa Omle, and Endre Kovacs. " The role of Roof Angle and Geographic Location on Thermal Performance of Buildings." International Journal of Thermofluids , under review (2025).

5. REFERENCES

[1] B. Chegari, M. Tabaa, E. Simeu, F. Moutaouakkil, and H. Medromi, "Multi-objective optimization of building energy performance and indoor thermal comfort by combining artificial neural networks and metaheuristic algorithms," *Energy Build*, vol. 239, p. 110839, 2021, doi: 10.1016/j.enbuild.2021.110839.

[2] I. International Energy Agency, "Energy Policy Review Hungary 2022," 2022.

[3] I. Beausoleil-Morrison, M. Kummert, F. MacDonald, R. Jost, T. McDowell, and A. Ferguson, "Demonstration of the new ESP-r and TRNSYS co-simulator for modelling solar buildings," *Energy Procedia*, vol. 30, pp. 505–514, 2012, doi: 10.1016/j.egypro.2012.11.060.

[4] J. E. Christian and J. Kosny, "Thermal performance and wall ratings," *ASHRAE J*, vol. 38, no. 3, Mar. 1996.

[5] D. Aelenei and F. M. A. Henriques, "Analysis of the condensation risk on exterior surface of building envelopes," *Energy Build*, vol. 40, no. 10, pp. 1866–1871, 2008, doi: 10.1016/J.ENBUILD.2008.04.003.

[6] J. Ji, C. Luo, W. Sun, H. Yu, W. He, and G. Pei, "An improved approach for the application of Trombe wall system to building construction with selective thermo-insulation façades," *Chinese Science Bulletin*, vol. 54, no. 11, pp. 1949–1956, Jun. 2009, doi: 10.1007/S11434-009-0353-6.

[7] L. Mátyás and I. F. Barna, "General Self-Similar Solutions of Diffusion Equation and Related Constructions," *Romanian Journal of Physics*, vol. 67, p. 101, 2022.

[8] T. Kusuda, "Fundamentals of building heat transfer," *J Res Natl Bur Stand (1934)*, vol. 82, no. 2, p. 97, 1977.

[9] M. K. Singh, S. Rajput, and R. K. Singh, "Study of 2D contaminant transport with depth varying input source in a groundwater reservoir," *Water Sci Technol Water Supply*, vol. 21, no. 4, pp. 1464–1480, Jun. 2021, doi: 10.2166/WS.2021.010/831257/WS2021010.PDF.

[10] A. H. Askar, I. Omle, E. Kovács, and J. Majár, "Testing Some Different Implementations of Heat Convection and Radiation in the Leapfrog-Hopscotch Algorithm," *Algorithms*, vol. 15, no. 11, p. 400, 2022.

[11] Á. Nagy, I. Omle, H. Kareem, E. Kovács, I. F. Barna, and G. Bognar, "Stable, explicit, leapfrog-hopscotch algorithms for the diffusion equation," *Computation*, vol. 9, no. 8, p. 92, 2021.

[12] C. Hirsch, *Numerical computation of internal and external flows, volume 1: Fundamentals of numerical discretization*. Wiley, 1988.

[13] I. Omle, A. H. Askar, and E. Kovács, "SYSTEMATIC TESTING OF EXPLICIT POSITIVITY PRESERVING ALGORITHMS FOR THE HEAT-EQUATION," 2022, doi: 10.28919/jmcs/7407.

[14] H. K. Jalghaf, E. Kovács, J. Majár, Á. Nagy, and A. H. Askar, "Explicit stable finite difference methods for diffusion-reaction type equations," *Mathematics*, vol. 9, no. 24, p. 3308, 2021.

[15] A. H. Askar, I. Omle, E. Kovács, and J. Majár, "Testing Some Different Implementations of Heat Convection and Radiation in the Leapfrog-Hopscotch Algorithm," *Algorithms*, vol. 15, no. 11, p. 400, 2022.

[16] A. H. Askar, Á. Nagy, I. F. Barna, and E. Kovács, "Analytical and Numerical Results for the Diffusion-Reaction Equation When the Reaction Coefficient Depends on Simultaneously the Space and Time Coordinates," *Computation*, vol. 11, no. 7, p. 127, 2023.

[17] A. H. Askar, E. Kovács, and B. Bolló, "Prediction and Optimization of Thermal Loads in Buildings with Different Shapes by Neural Networks and Recent Finite Difference Methods," *Buildings*, vol. 13, no. 11, p. 2862, 2023.

[18] A. H. Askar, I. Omle, and E. Kovács, "The role of roof angle and geographic location on the thermal performance of buildings," *International Journal of Thermofluids*, vol. 27, p. 101192, May 2025, doi: 10.1016/J.IJFT.2025.101192.

[19] A. A. Habeeb, K. Endre, and B. Betti, "Multi objective optimization for house roof using artificial neural network model," *Multidiszciplináris Tudományok*, vol. 13, no. 2, pp. 11–25, 2023.